Solidification of supercooled water in the vicinity of a solid wall

Markus Schremb* and Cameron Tropea
Institute of Fluid Mechanics and Aerodynamics, Technische Universität Darmstadt, 64289 Darmstadt, Germany
(Received 30 August 2016; published 9 November 2016)

An experimental approach utilizing a Hele-Shaw cell for the investigation of the solidification of a supercooled liquid in contact with a solid wall is presented. The setup is based on an idea presented by Marín *et al.* [A. G. Marín *et al.*, Phys. Rev. Lett. **113**, 054301 (2014)], who investigated the planar freezing of a sessile drop without supercooling. This apparatus overcomes optical distortions present when observing the freezing of sessile drops, arising due to reflections and refraction of light on the drop surface. The facility is used to investigate the freezing process of water drops, supercooled down to -20° C, and to qualitatively demonstrate that the growth behavior is uninfluenced by the use of the Hele-Shaw cell. Different features during freezing, which are known for sessile water drops, are also observed with the Hele-Shaw cell. The growth morphology within the first phase of solidification is categorized according to the initial drop supercooling. Furthermore, freezing velocities within this phase are related to data available in the literature for the growth of single ice dendrites.

DOI: 10.1103/PhysRevE.94.052804

I. INTRODUCTION

Icing of solid structures is ubiquitous in nature and on synthetic structures and may occur due to resublimation from the vapor phase, i.e., frost formation [1–3], the impact and accretion of liquid, supercooled drops [4,5], or ice particles [6], or due to the freezing of drops at rest on a solid surface [7–14]. While the reasons for icing are manifold, freezing drops often represent a hazard for transportation systems, such as aviation, shipping [15,16], and road traffic [17], but also affect the operational reliability of power supply systems [18]. Therefore, understanding the mechanisms during icing of surfaces is of utmost importance.

Numerous studies exist concerning the solidification of a sessile drop or a liquid in general, where the focus has typically been on the macroscopic behavior, such as the shape evolution during freezing [7,9,10,12,13], the influence of the surface wettability [19–21], and surface roughness or structure [22,23] on the freezing delay time, or the qualitative description of the solidification process from a supercooled state [8,14,24,25]. Related to the latter aspect, an experimental facility is introduced enabling the investigation of the interaction between a solidifying supercooled drop and the surface below the drop. It offers qualitative and quantitative insights into the basic mechanisms taking place during solidification. Different ice growth modes and characteristic speeds of solidification, both depending on the liquid's degree of supercooling, are identified and quantified. The main feature of the facility is that the sessile drop is effectively only two dimensional and the dendrite or freezing front propagation can be captured with high contrast using the planar image of a high-speed camera.

II. EXPERIMENTAL FACILITY AND METHOD

The experimental facility consists of a cooling system, a vertically oriented Hele-Shaw cell, and an optical system. A cooling plate capable of maintaining a specified temperature by an external chiller is used for the experiments and allows plate temperatures down to -30° C. The plate is placed in a closed styrofoam chamber. To prevent the buildup of frost and condensate on the cold surfaces, the environment within the chamber is kept dry by the use of gaseous nitrogen. A double-glass side window provides optical access to the styrofoam chamber. The Hele-Shaw cell with an inserted drop is pictured in Fig. 1. As shown in the figure, the drop is trapped between two sheets of plexiglass, and a strip of copper, which maintains a constant distance of 1 mm between the sidewalls, serves as the substrate on which the drop is at rest. The combination of the sidewalls and the substrate strip are stacked and fixed by screws within an aluminum base. The temperature of the drop is measured with a thermocouple immersed into the copper, ending approximately 0.5 mm below the substrate's surface under the drop. For high thermal conductivity materials like copper, the temperature gradient in the substrate region between the drop and the thermocouple's tip is negligible and the drop's base can be assumed to be at the temperature measured within the substrate.

The freezing process is observed with a high-speed video camera (Photron MC 2.1), operated at a frame rate of 2000 frames/s with a resolution of 512×256 pixels^2. The process is captured with a spatial resolution of approximately 13 μm/pixel. With an illuminated diffusor screen behind the Hele-Shaw cell, the freezing process is captured in the form of backlight shadowgraph videos.

At the beginning of each experiment, the Hele-Shaw cell with an entrapped drop, both at room temperature, are placed onto the cooling plate, which is precooled to 0° C. Afterward, the cooling plate is cooled down at a moderate cooling rate of approximately 0.2 K/s, resulting in a simultaneous cooldown of the substrate and the drop. Based on the recalescence during the first phase of solidification, the temperature at the moment of freezing is obtained as the lowest value before the steep rise of the temperature signal, corresponding to freezing at the substrate surface. Drops of varying volumes ranging between 1.5 and 10 μl and diameters between 2 and 5 mm have been used and no correlation between the drop volume and the freezing process has been observed.

*schremb@sla.tu-darmstadt.de

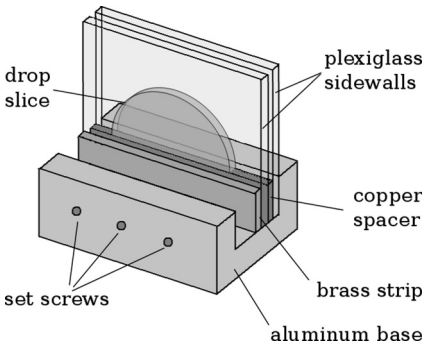

FIG. 1. Schematic of the Hele-Shaw cell with inserted drop.

III. RESULTS AND OBSERVATIONS

It is commonly known that the freezing process of a supercooled liquid can be subdivided into two phases.

(i) During the first phase of solidification, the supercooled liquid departs from the thermodynamic metastable state, resulting in a mixture of liquid and solid at the melting temperature, which is referred to as the recalescence phase [26].

(ii) During the second phase of solidification, the remaining liquid in the solid-liquid mixture solidifies in a thermodynamically stable state at the melting temperature.

These phases are distinctly captured using the present facility.

A. First phase of supercooled freezing

Figure 2 shows the first 22 ms of the solidification of a supercooled sessile water drop. While the process observed in the Hele-Shaw cell is depicted in the top row, the bottom row of Fig. 2 shows the same process observed for a sessile drop. The direct comparison indicates that the overall process is the same in both cases, differing only in the visibility. In the case of the sessile drop, the curved drop interface causes reflections and refraction, resulting in low contrast of the different regions within the drop. Furthermore, the exact location of nucleation and the direction of the solidification cannot be clearly determined from the high-speed videos. In the case of the drop within the Hele-Shaw cell, these optical distortions are suppressed and the solidification process and the resulting phase distribution are clearly visible.

The sequences in Fig. 2 show the first phase of solidification or the recalescence phase. Nucleation starts at an arbitrary point of the solid substrate in the form of heterogeneous nucleation and is followed by a rapid kinetic crystal growth. It is driven by the initial liquid supercooling and leads to the growth of a microscopic dendritic ice structure, filling out the entire volume of the liquid. The process is accompanied by a warming up of the solid-liquid mixture to the equilibrium freezing temperature until the initial supercooling is exhausted. Therefore, the degree of supercooling determines the portion f of the liquid that is frozen after this first stage.

Considering the freezing of a thermally insulated volume of supercooled liquid at temperature T, the latent heat of freezing equals the sensible heat of warming up the solid-liquid mixture as $fL = c_p(T_m - T)$, where L, c_p, and T_m are the liquid's latent heat of fusion, heat capacity, and equilibrium freezing temperature, respectively [28]. Therefore, the solid fraction f is given as

$$f = \frac{c_p(T_m - T)}{L}, \tag{1}$$

which is commonly referred to as the Stefan number St. When the supercooling is exhausted and the solid-liquid mixture is in thermodynamic equilibrium at T_m, a further removal of heat results in continued freezing of the remaining liquid entrapped within the dendritic ice structure. In this case, the growth direction of the solid-liquid interface is at each point in the direction opposite to the heat flux.

B. Second phase of supercooled freezing

The processes involved in the second phase of solidification are shown in Fig. 3, again for the Hele-Shaw cell (top row) and a sessile drop (bottom row). After the first phase of solidification has finished, the drop consists of a solid-liquid mixture in thermodynamical equilibrium at $T = T_m$. Due to continued cooling by the substrate, the remaining liquid freezes, beginning at the substrate's surface. In accordance with the explanations above, the growth direction in the beginning of the second phase of solidification is normal to the substrate's surface, i.e., in the negative direction of the heat flux into the substrate. It has been shown that the freezing front within a sessile drop becomes curved due to a boundary constraint at the three-phase contact line of ice, water, and air [7,9,10,12,13], namely, that the freezing front is perpendicular to the liquid-gas interface. So far, this effect has been observed

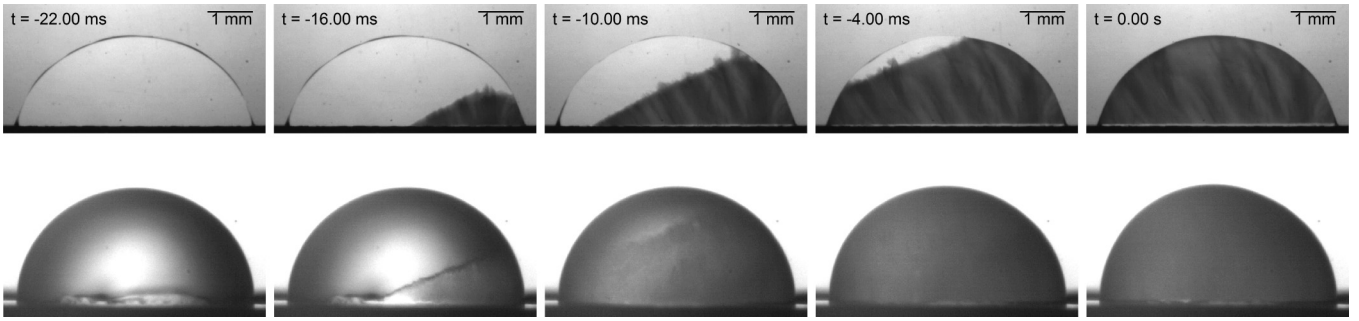

FIG. 2. First phase of solidification of a water drop, supercooled to approximately -15.8° C [27]. Qualitative comparison of a drop within the Hele-Shaw cell (top row) with a sessile drop (bottom row).

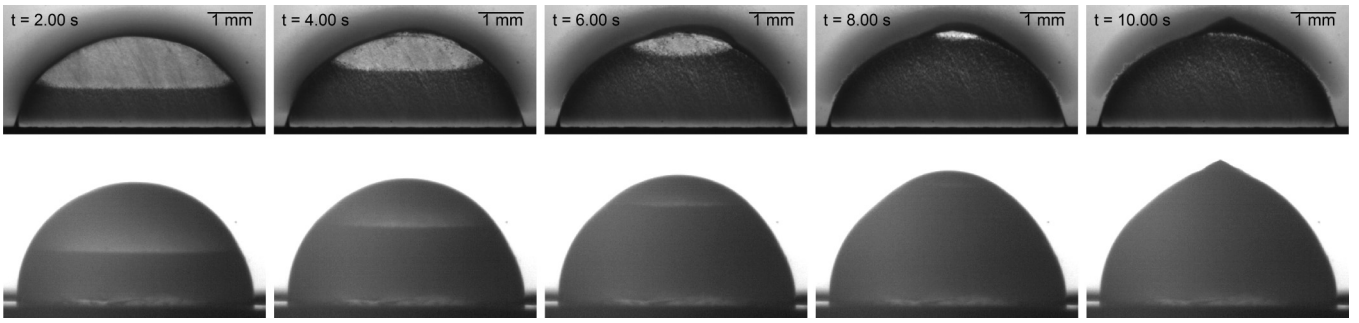

FIG. 3. Second phase of solidification of the supercooled drops of Fig. 2 [27]. According to Eq. (1), approximately 19% of the liquid is already frozen at the beginning of this stage. The top row shows a drop in the Hele-Shaw cell and the bottom row a sessile drop.

within sessile drops freezing at T_m without any supercooling. Here it is shown that the condition also holds for a drop in which just the remaining liquid within a dendritic structure of ice solidifies (Fig. 3).

While the curved freezing front is difficult to observe in the case of the sessile drop, it can be clearly seen with the Hele-Shaw setup. As shown in the figure, for both the sessile drop and the drop within the Hele-Shaw cell, the second phase of freezing results in a cusp shape on top of the frozen drop. This is due to the above-mentioned boundary constraint at the ice-water-air contact line, accompanied by the density decrease and volume expansion during freezing, which finally results in the observable shape. This phenomenon was only reported for the case of a drop that freezes without initial supercooling [7,10,12,13]; the same behavior is observable during the second phase of freezing of a supercooled drop and also for a drop in the Hele-Shaw cell.

During the evolution of this cusp shape, the first qualitative difference between the freezing behavior of a sessile drop and the planar one arises, namely, the position of the cusp on the frozen drop. Since the freezing process and all influential effects are axisymmetric in the case of the sessile drop, the cusp is formed in the middle on top of the drop (north pole). In the case of the drop in the Hele-Shaw cell, the cusp does not appear in the symmetry plane of the drop due to the additional forces acting between the liquid meniscus and the plexiglass sidewalls. An uneven surface of the sidewalls may lead to local pinning of the contact line, resulting in a nonuniform contact line movement during volume expansion and finally an asymmetric shape of the frozen drop.

Another qualitative difference of the overall behavior within the Hele-Shaw cell compared to that of the sessile drop can be seen in Fig. 3. After the first phase of solidification, the solid-liquid mixture is instantaneously at the melting temperature, while the plexiglass sidewalls are still at the initial temperature of the drop. As described by Jung *et al.* [8] for freezing sessile supercooled water drops, the fast recalescence of the drop during the first freezing phase causes the air around the drop to be supersaturated with respect to the initial drop temperature. This supersaturation leads to a condensation halo on the plexiglass sidewalls around the drop. Since the frozen part of the drop is cooled down again below the freezing temperature of water by the ongoing cooling of the substrate, the supersaturation around the drop decreases. As a consequence, starting from the substrate, the condensation halo again dissolves.

C. Solidification at a solid wall

The above-mentioned two phases of solidification are well known and described for the case of a supercooled drop freezing without the influence of a neighboring substrate. Kong and Liu [24] investigated the solidification of supercooled water in the vicinity of a solid substrate with water temperatures down to approximately -7° C and varying substrate materials. They captured the solidification at the substrate with two high-speed video cameras for a top view and a side view and observed a further process taking place before the two phases of solidification described above. They triggered nucleation at a point on the substrate and found that the subsequent freezing process starts with the propagation of a thin ice layer over the substrate's surface. This is also observed in the initial freezing stage in the Hele-Shaw cell as a moving bright region next to the substrate [27].

According to Kong and Liu [24], for water temperatures above 270 K the ice growth parallel to the surface is followed by the growth of ice normal to the surface, representing an increase of the thickness of the initial ice layer. However, in the case of water temperatures below 270 K, Kong and Liu observed that the thin ice layer on top of the substrate becomes unstable at a certain point behind the moving three-phase contact line (of ice, water, and substrate) of the propagating layer, resulting in the growth of dendritic ice into the bulk of the liquid. For the range of relatively low supercooling, they observed single dendrites and hexahedral shapes of ice crystals emerging from the initial ice layer on the substrate. In the present study we observed the process for larger liquid supercoolings of up to 20 K. We found that not only is there a temperature transition between the cases of purely planar and dendritic ice growth within the bulk, but there are also several transitions between different growth modes of dendritic growth.

The different growth modes are categorized in Table I and can be described as follows. As already observed by Kong and Liu [24] and described above, for low supercoolings, the initial ice layer remains stable and its thickness increases by planar growth normal to the substrate's surface. In this case, the presented first phase of supercooled solidification is not observable. While Kong and Liu [24] mentioned a threshold of approximately $\Delta T = 2.6$ K, we found the transition to occur at approximately $\Delta T = 4.7$ K. For larger supercooling between approximately $\Delta T = 4.7$ and 7.2 K, the ice layer becomes unstable long after the growth of the initial ice layer, when the layer has already covered a large part of the wetted substrate.

TABLE I. Different freezing regimes of the first phase of supercooled solidification for different supercooling. The initial ice layer moves from the right to the left and its front is at the left side of each photograph. Inserted vertical lines mark the position of first visible instabilities.

Description	Supercooling (K)	Detail
Planar	0, . . . ,4.7	
Late dendrites	4.7, . . . ,7.2	
Single dendrites	7.2, . . . ,9.9	
Inhomogeneous front	9.9, . . . ,12.0	
Homogeneous front	12.0, . . .	

As observed by Kong and Liu [24], this instability results in the growth of single dendrites and hexahedral ice crystals. If the supercooling is in the range of approximately $\Delta T = 7.2, \ldots, 9.9$ K, many more single dendrites and hexahedral ice crystals emerge from the ice layer than in the case of lower supercooling. The time of their occurrence after the initial ice layer growth is much shorter, i.e., they appear closer behind the front of the initial ice layer (compare photographs in Table I). For the supercooling range of approximately $\Delta T = 9.9, \ldots, 12.0$ K, not only single dendrites but a mesh of dendrites evolves at a small distance behind the moving contact line. In this case, the dendrites' orientations are random, resulting in an inhomogeneous distribution of the ice. If the supercooling is even higher, with $\Delta T > 12.0$ K, the dendrites are all oriented parallel, leading to a homogeneous ice distribution after the first phase of solidification, as shown in Fig. 2. The dendrites all grow at the same speed, resulting in the parallel propagation of a relatively smooth envelope of the mushy region.

The front velocity v_f through the drop's bulk is plotted as a function of the supercooling in Fig. 4. Depending on the liquid's supercooling and according to the categorization in

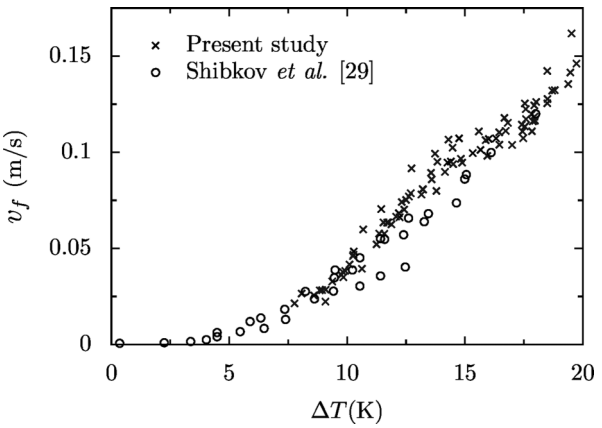

FIG. 4. Freezing velocity within the bulk liquid as a function of the liquid supercooling. Depending on supercooling, this velocity represents the dendrite tip velocity or that of the envelope of the mushy region. Comparison with results for a single dendrite tip by Shibkov *et al.* [29].

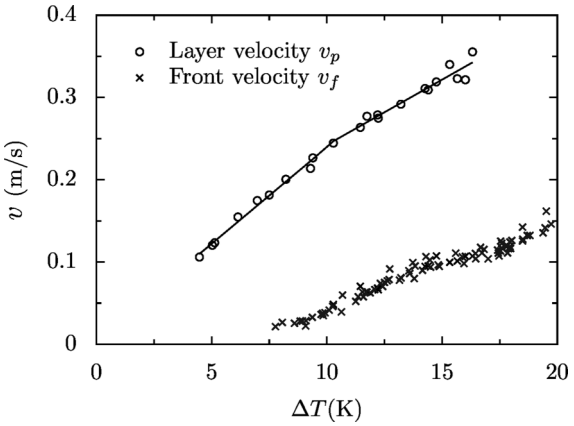

FIG. 5. Initial ice layer velocity parallel to the substrate's surface as a function of the liquid's supercooling. Comparison with the front velocity within the bulk.

Table I, it represents the velocity of the dendrite tips, or the normal velocity of the mushy region envelope. For comparison purposes, the tip velocity of a freely growing single dendrite, experimentally obtained by Shibkov *et al.* [29], is also shown in Fig. 4. For lower supercooling of up to approximately $\Delta T = 10$ K, the front velocity within our experiments compares very well with that of a single dendrite. In this temperature range, the influence of neighboring dendrites on the growth speed of an individual dendrite is negligible, as already shown numerically by Criscione *et al.* [30].

For supercooling above 10 K, the front velocity within our experiments is slightly higher than that of a single dendrite, representing a small thermal influence between the propagating dendrites. This temperature was found before as the threshold subdividing the regimes of single dendrite propagation and inhomogeneous front propagation within the bulk liquid (see Table I). In the case of larger supercooling, the influence of kinetic effects during molecular attachment at the water-ice interface on the dendrite tip velocity increases. While this effect plays an important role for supercooling above approximately 4–5 K in the case of a single dendrite [29], it becomes important at approximately $\Delta T > 14$ K for our experiments. For even higher supercooling, the growth velocity of a single dendrite and the front velocity observed within the present study compare very well again. Since the effect of neighboring dendrites on the growth of an individual dendrite is presumably only of thermal nature, this behavior of the growth velocities for higher supercooling indicates that the growth is dominated by kinetic effects in the range of high supercooling.

The layer velocity v_p of the initial ice layer parallel to the substrate surface as a function of the supercooling is shown in Fig. 5. For comparison purposes, the measured front velocity v_f is also shown. The layer velocity is well represented by a linear relation up to a supercooling of $\Delta T \approx 10$ K. For higher supercooling, the slope of this dependence decreases, but remains linear. The decreasing slope is probably due to kinetic effects. It should be emphasized here that this change of slope of the linear relation coincides with the threshold between the propagation of single dendrites and an inhomogeneous front within the bulk liquid. The velocity of the ice layer front

parallel to the substrate surface is much higher than the velocity of the dendrite front within the bulk liquid.

As shown by Kong and Liu [24], besides temperature, the layer velocity at the substrate depends also on the substrate's thermal properties. Schremb *et al.* [4] investigated the freezing of water drops, initially at room temperature, impacting a cold aluminum surface. They observed the process in a top view and measured the velocity of the dendritic front propagating through the spread out water drops. Due to the top view observation, they did not measure the normal front velocity v_f within the bulk liquid, but rather the velocity of the intersection line of the dendritic front with the impact surface, which represents the velocity of the initial ice layer v_p. Based on the contact temperature at the substrate surface, calculated according to [31], they estimated the drop temperature, which is relevant for the freezing process, to be -14.7° C, and measured a velocity of 0.32 m/s. In contrast to Schremb *et al.* [4], a different substrate material, namely, copper, is used in the present study, but also a layer velocity of 0.32 m/s for a given supercooling of -14.7° C is obtained. Kong and Liu [24] found a strong dependence of the layer velocity on the substrate's properties for a supercooling of up to 7 K. However, the comparison of the present results with the measured velocity of Schremb *et al.* [4] suggests that there is only a weak dependence on the substrate's properties in the case of higher supercooling, at least when comparing high thermal conductivity materials like copper and aluminum.

IV. CONCLUSION

An experimental approach for the investigation of the freezing process of sessile supercooled water drops has been presented. By making use of a Hele-Shaw cell, into which a drop is inserted, this method allows observation of the process in a quasi-two-dimensional manner, without optical distortions arising from the drop's free surface. Thereby, the visibility of the process in terms of contrast and optical distortions is enhanced. The freezing process of water drops supercooled down to -20° C has been captured with a high-speed video system.

It has been qualitatively shown that the freezing process within the Hele-Shaw cell is the same as in a free sessile drop. Findings by Kong and Liu [24] concerning the freezing process of a supercooled melt next to a solid substrate have been confirmed, namely, before the two phases of solidification, an ice layer propagates over the substrate's surface. For large supercooling, this layer becomes unstable, resulting in different modes of dendritic growth. We have categorized these growth modes according to the liquid's supercooling. Freezing velocities of the initial ice layer and the ice propagating through the drop's bulk have been analyzed and compared to available experimental data of freezing processes within a liquid at rest or during drop impact. We have found that there is no difference of the propagation velocity of multiple dendrites compared to that of a single dendrite in the case of low supercooling. For higher supercooling, a small mutual influence of the dendrites is observed, as long as the freezing process is dominated by heat diffusion. For even higher supercooling, when the process is dominated by kinetic effects, there is no mutual influence of the dendrites and the normal growth velocity of a dendritic front again equals that of a single dendrite.

Kong and Liu [24] found a crucial influence of the substrate's thermal properties on the growth velocity of the initial ice layer parallel to the surface, at least for the observed range of supercooling of up to 7 K. However, a comparison of growth velocities obtained within the present study to the growth velocity measured by Schremb *et al.* [4] for an impacting drop suggests that the substrate's influence on the growth velocity is negligible for higher supercooling. The initial ice layer is in direct contact with the substrate below the drop and presumably mechanically interlocking with it during the freezing process. Furthermore, the ice layer's growth velocity is the velocity that determines how fast a surface is covered by ice and therefore it is the most relevant freezing velocity for the case of icing of surfaces. Hence, future studies should focus on the influence of the substrate's properties on the speed of the initial ice layer, especially in the case of higher supercooling.

ACKNOWLEDGMENTS

We gratefully acknowledge financial support from the Deutsche Forschungsgemeinschaft within the collaborative research Project No. SFB-TRR 75 (TP-C3). Furthermore, we thank S. Iannella for her contribution to the design of the setup and conducting the first experiments within the scope of her Masters thesis and Ilia V. Roisman for some useful discussions about the topic.

[1] R. W. Style, The formation and evolution of frost flowers and related phenomena, Ph.D. thesis, University of Cambridge, 2007.

[2] D. A. Ali and R. R. Crawford, The effects of frost formation on the performance of domestic refrigerator-freezer finned-tube evaporator coils, ACRC Tech. Rep. 15, Air Conditioning and Refrigeration Center, University of Illinois, Urbana, IL, 1992.

[3] S. Jung, M. K. Tiwari, and D. Poulikakos, Proc. Natl. Acad. Sci. USA **109**, 16073 (2012).

[4] M. Schremb, I. V. Roisman, and C. Tropea, *Proceedings of the 13th Triennial International Conference on Liquid Atomization and Spray Systems* (National Cheng Kung University, Tainan, Taiwan, 2015).

[5] M. Schremb, I. V. Roisman, S. Jakirlić, and C. Tropea, *Proceedings of the 27th Annual Conference on Liquid Atomization and Spray Systems* (University of Brighton, Brighton, UK, 2016).

[6] J. G. Mason, J. W. Strapp, and P. Chow, Proceedings of the 44th AIAA Aerospace Sciences Meeting, Reno, 2006.

[7] W. W. Schultz, M. G. Worster, and D. M. Anderson, in *Interactive Dynamics of Convection and Solidification*, edited by P. Ehrhard, D. S. Riley, and P. H. Steen (Kluwer, Dordrecht, 2001), pp. 209–226.

[8] S. Jung, M. K. Tiwari, N. V. Doan, and D. Poulikakos, Nat. Commun. **3**, 615 (2012).
[9] O. R. Enríquez, Á. G. Marín, K. G. Winkels, and J. H. Snoeijer, Phys. Fluids **24**, 091102 (2012).
[10] A. G. Marín, O. R. Enríquez, P. Brunet, P. Colinet, and J. H. Snoeijer, Phys. Rev. Lett. **113**, 054301 (2014).
[11] J. H. Snoeijer and Brunet, Am. J. Phys. **80**, 764 (2012).
[12] M. Nauenberg, Eur. J. Phys. **37**, 045102 (2016).
[13] M. Nauenberg, arXiv:1404.4425.
[14] F. Tavakoli, S. H. Davis, and H. P. Kavehpour, J. Coatings Technol. Res. **12**, 869 (2015).
[15] J. R. Stallabrass, *Methods for the Alleviation of Ship Icing* (National Research Council of Canada, Ottawa, Canada, 1970).
[16] C. C. Ryerson and A. J. Gow, *Ship Superstructure Icing: Crystalline and Physical Properties*, Tech. Rep. ERDC/CRREL TR-00-11, Cold Regions Research and Engineering Laboratory (Engineer Research and Development Center, Hanover, NH, 2000).
[17] L. Symons and A. Perry, Meteor. Appl. **4**, 17 (1997).
[18] M. E. Farzaneh, *Atmospheric Icing of Power Networks* (Springer Science & Business Media, New York, 2008).
[19] A. Alizadeh, M. Yamada, R. Li, W. Shang, S. Otta, S. Zhong, L. Ge, A. Dhinojwala, K. R. Conway, V. Bahadur, A. J. Vinciquerra, B. Stephens, and M. L. Blohm, Langmuir **28**, 3180 (2012).
[20] L. Boinovich, A. M. Emelyanenko, V. V. Korolev, and A. S. Pashinin, Langmuir **30**, 1659 (2014).
[21] P. Tourkine, M. Le Merrer, and D. Quere, Langmuir **25**, 7214 (2009).
[22] J. M. Campbell, F. C. Meldrum, and H. K. Christenson, J. Phys. Chem. C **119**, 1164 (2015).
[23] P. Eberle, M. K. Tiwari, T. Maitra, and D. Poulikakos, Nanoscale **6**, 4874 (2014).
[24] W. Kong and H. Liu, Int. J. Heat Mass Transfer **91**, 1217 (2015).
[25] S. V. Alekseenko, C. Mendig, M. Schulz, M. Sinapius, and O. A. Prykhodko, Tech. Phys. Lett. **42**, 524 (2016).
[26] J. P. Hindmarsh, A. B. Russell, and X. D. Chen, Int. J. Heat Mass Transfer **46**, 1199 (2003).
[27] See Supplemental Material at http://link.aps.org/supplemental/10.1103/PhysRevE.94.052804 for videos of freezing sessile water drops.
[28] L. Makkonen, Appl. Phys. Lett. **96**, 091910 (2010).
[29] A. Shibkov, Y. Golovin, M. Zheltov, A. Korolev, and A. Leonov, Physica A **319**, 65 (2003).
[30] A. Criscione, I. V. Roisman, S. Jakirlić, and C. Tropea, Int. J. Thermal Sci. **92**, 150 (2015).
[31] M. Seki, H. Kawamura, and K. Sanokawa, J. Heat Transfer **100**, 167 (1978).